# Inverse Procedural Modeling of Knitwear (Supplemental Material)

Elena Trunz, Sebastian Merzbach, Jonathan Klein, Thomas Schulze, Michael Weinmann, Reinhard Klein
Institute of Computer Science II, University of Bonn, Germany
{trunz,merzbach,kleinj,mw,rk}@cs.uni-bonn.de, s6tsschu@uni-bonn.de

## 1. Overview

The workflow of our approach is outlined in Figure 1. An initial (optional) pre-processing step compensates for non-axis-alignment of the depicted knit patterns. This allows handling tilted images of knitwear in our framework. In the next step, the user provides exemplars of particular basic stitch types, such as knits or purls within the image via an intuitive interface. Subsequently, hypotheses regarding the coarse localization of the individual stitch types are derived based on searching image patches containing the respective stitch types within the whole image. This serves as an initialization for the inference of the underlying grid structure, which is performed in the next step of the pipeline. During an error correction step to handle misclassified stitch types in the grid, we simultaneously perform the detection of the size of the repeating pattern. The final step is the derivation of the underlying production rules and their conversion into corresponding knitting instructions (in analogy to the depictions in knitting books). These rules allow the reproduction of the knitting pattern depicted in the input image.

## 2. Running Times and Problem Sizes

Table 1 provides an overview over the problem sizes and computation times for the examples shown in this supplemental material (see Figure 9 for **sample IDs 1, 2, 3, 4**, Figure 2 for **sample ID 5** and Figure 3 for **sample ID 6**).

There is evidence that with an increasing problem size, the computational times increase drastically. The computation times required for solving the corresponding ILP can be significantly reduced by downsampling the likelihood maps obtained from the extended BBS template matching [1]. As demonstrated in Figure 2, a rescaling by the factor of 0.5 yields still similar results for the inferred grid structure at significantly shorter processing time.

## 3. Pre-processing

Figure 8 demonstrates the pre-processing step of our approach, which compensates for a possible non-axis-alignment of the input image.

Table 1: Problem sizes and resulting running times: The columns contain the image size (IS), the running times (in seconds) of BBS (extended with additional gradient information, as explaned in the paper), the downscaling factor for the likelihood maps (S), the running times of the ILP as well as the size of both the grid (GS) and the pattern (PS). $e_G$ and $e_P$ denote the fraction of misclassified stitch types for the overall grid and the pattern after error correction.

| ID | IS | BBS | S | ILP | GS | PS | $e_G$ | $e_P$ |
|---|---|---|---|---|---|---|---|---|
| 1 | 558× 300 | 202.91 | 0.5 | 6.75 | 7×5 | 2×2 | 0 | 0 |
| 1 | 558× 300 | 202.91 | 1 | 156.78 | 7×5 | 2×2 | 0 | 0 |
| 2 | 322× 299 | 37.46 | 0.25 | 0.22 | 5×7 | 1×2 | 0 | 0 |
| 2 | 322× 299 | 37.46 | 0.5 | 3.59 | 5×7 | 1×2 | 0 | 0 |
| 2 | 322× 299 | 37.46 | 1 | 70.12 | 5×7 | 1×2 | 0 | 0 |
| 3 | 684×413 | 99.62 | 0.5 | 10.03 | 10×9 | 5×4 | 2/90 | 0 |
| 3 | 684×413 | 99.62 | 1 | 264.18 | 10×9 | 5×4 | 2/90 | 0 |
| 4 | 1154×784 | 1103.46 | 0.5 | 103.59 | 16×15 | 7×7 | 11/240 | 0 |
| 5 | 529×214 | 18.10 | 0.5 | 3.10 | 10×6 | 4×2 | 0 | 0 |
| 5 | 529×214 | 18.10 | 1 | 72.07 | 10×6 | 4×2 | 0 | 0 |
| 6 | 885×207 | 118.84 | 0.5 | 11.93 | 11×3 | 5×1 | 0 | 0 |
| 6 | 885×207 | 118.84 | 1 | 292.38 | 11×3 | 5×1 | 0 | 0 |
| 7 | 687×171 | 44.94 | 0.5 | 6.21 | 10×3 | 8×1 | 3/30 | 0 |

## 4. Susceptibility to Template Selection

As stated in the paper, to evaluate the robustness regarding the selection of templates for the individual stitch types, we performed a study where 10 people aged between 10 and 67 years were asked to provide respective annotations. Ten samples of each stitch type (knit and purl), similar to the ones depicted in Figure 1 of the paper, were shown to each participant. Finally the participants were asked to select one sample of each type in the input image, whereby they were asked to select respective templates that contained complete stitches. Using these different stitch templates, we infer the respective grid structure using our framework. Some of the selections and the corresponding grids are shown in Figure 3.

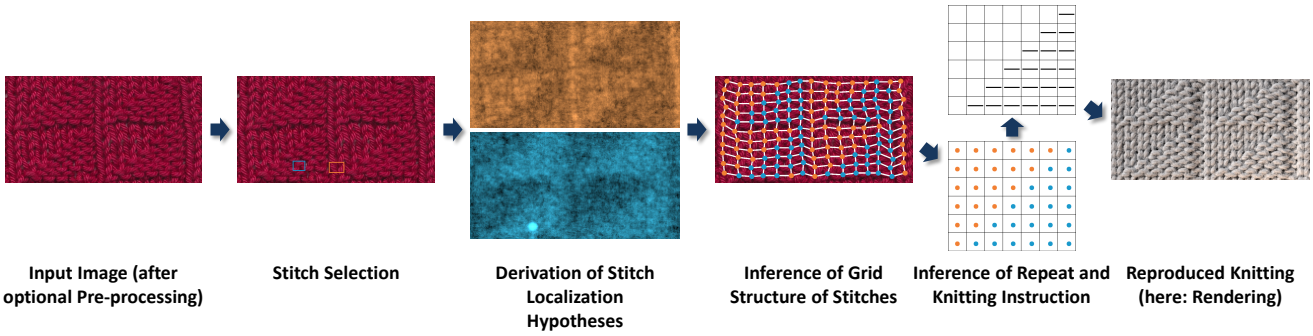


Figure 1: Overview of the proposed pipeline.

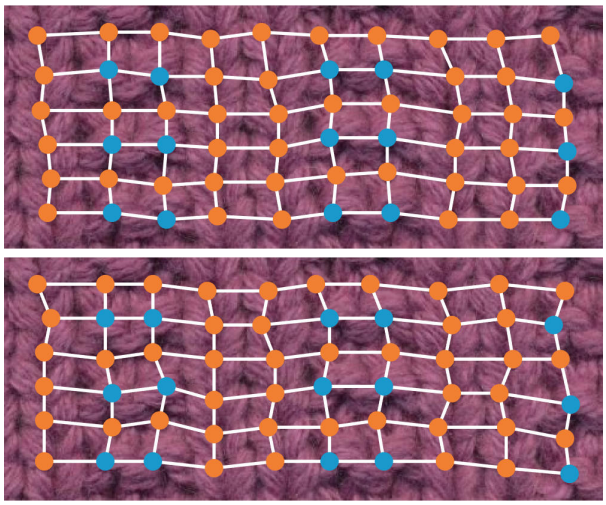

Figure 2: The resulting grid after the optimization step without resizing the likelihood maps (top) and with a resizing by a factor of 0.5 (bottom). **Sample ID 5**.

## 5. Computation of Row and Column Number for Optimization

Figure 4 illustrates the typical result for the estimation of the number of columns $c$ and rows $r$ based on one template according to the pre-computation of the grid size for the optimization (see Section 4.4.2 in the paper). The rectangles represent the templates for the knit (orange) and purl (blue) stitch provided by the user. The same procedure is repeated for the other template. As stated in the paper, the strips extracted from this step are analyzed to estimate uncertainties in the spatial extensions of the stitches (see Figure 5), which are then used for the optimization.

## 6. Distance Measure

In order to evaluate the distance measure which was used to find a pattern size and to correct the errors of stitch labelings, we considered four scenarios illustrated in Figure 6. First the minimal distance was computed for a pattern (which was detected from the grid in Figure 3) without recognition errors. Afterwards, we added 3%, 7%, and 11% random recognition errors respectively and evaluated the minimal distance again. We simulated this procedure several times and observed that our Hamming distance based measure is robust against moderate recognition errors. Only when the pattern is not recognizable due to a very high amount of errors, our error correction procedure may fail

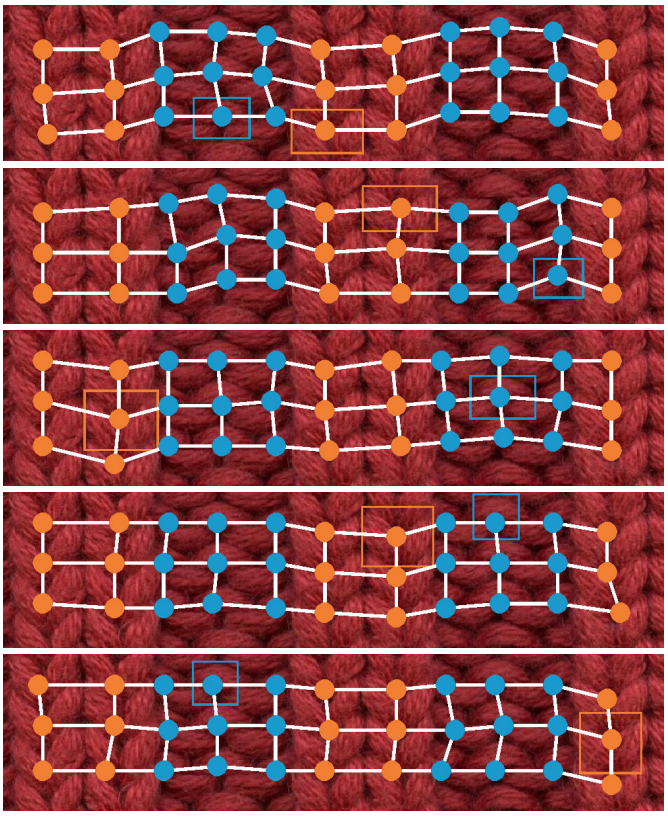

Figure 3: Examples of different template selections and the resulting grids. **Sample ID 6** (top).

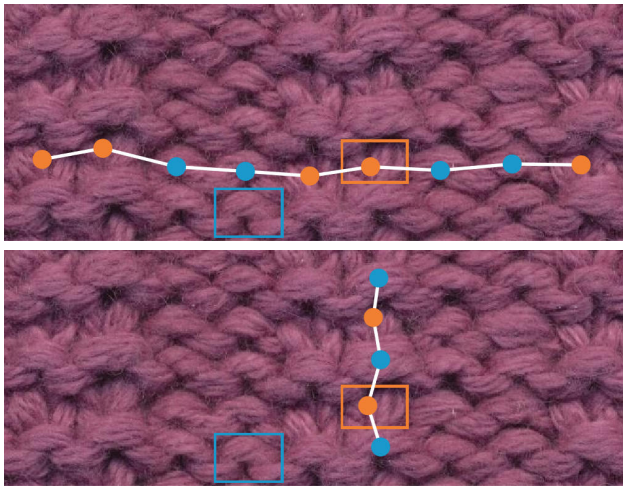

Figure 4: Detected number of rows and columns.

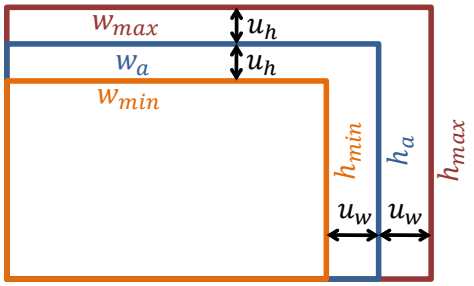


Figure 5: Average stitch width $w_a$ and height $h_a$, and uncertainties $u_w$, $u_h$ for different spatial extensions of stitches.

to find the correct size of the repeat.

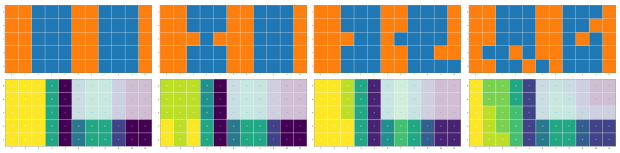

Figure 6: Evaluation of the distance measure used to find the correct size of the repeating pattern and to correct the errors of stitch labelings. Entries with faded colors represent stitch sizes discarded during the error correction procedure. Cells with a dark blue colorization denote adequate pattern sizes.

## 7. Comparison of the Extracted Repeat Pattern

We additionally provide an example for the extraction of an as intuitive as possible repeating pattern from the underlying grid structure. While an appropriate size of the repeating pattern can be reliably detected by the error correction and pattern extraction step (see Section 4.5 of the paper), the exploitation of the law of Prägnanz additionally allows the extraction of a repeat without breaking existing structures within the pattern such as triangles (see Figure 7 (left)).

Figure 7: The left image represents the pattern repeat found by our algorithm based on the law of Prägnanz. This pattern repeat is intuitive in the sense that the triangular structure is preserved. In comparison, other ”shifted“ repeat patterns (middle and right) of the same size appear not as ”intuitive“ as human observers cannot infer the underlying pattern that easily.

## 8. Example with Three Stitch Types

To demonstrate the ability of our method to deal with more than two stitch types, we provide a respective example with three stitch types in Figure 10. Here, the stitch types used in other examples (i.e. purl and (straight) knit) are accompanied by a further type denoted as twisted knit. As a consequence, the user provides three templates (marked in green for twisted knit, orange for straight knit and blue for purl) that are used to derive the likelihood maps. These are used to infer the grid structure (including three stitch types).

## References

[1] T. Dekel, S. Oron, M. Rubinstein, S. Avidan, and W. T. Freeman. Best-buddies similarity for robust template matching. In *2015 IEEE Conference on Computer Vision and Pattern Recognition (CVPR)*, pages 2021–2029, June 2015.

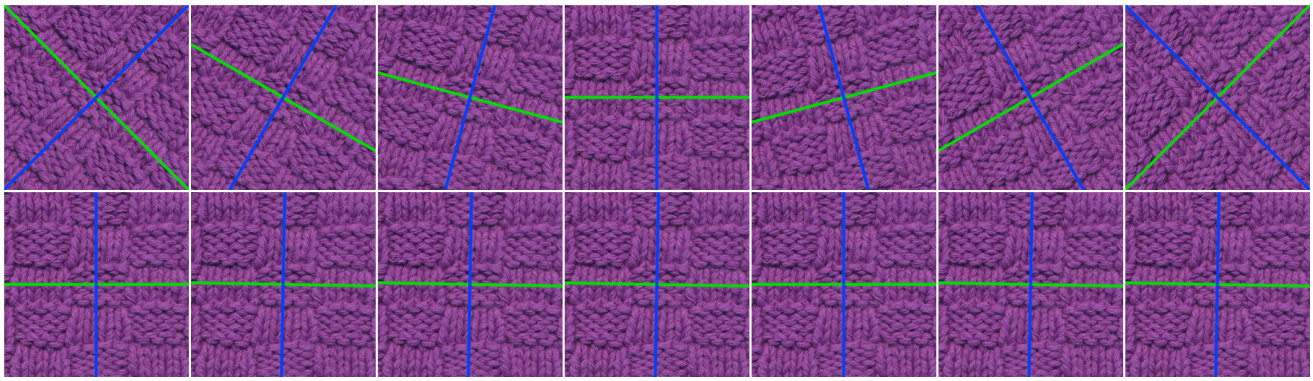

Figure 8: Automatic axis alignment using HOG in case of severe mis-alignments: The colored lines denote the dominant gradient orientations and are used to align the input images (top row) with respect to the axes (bottom row).

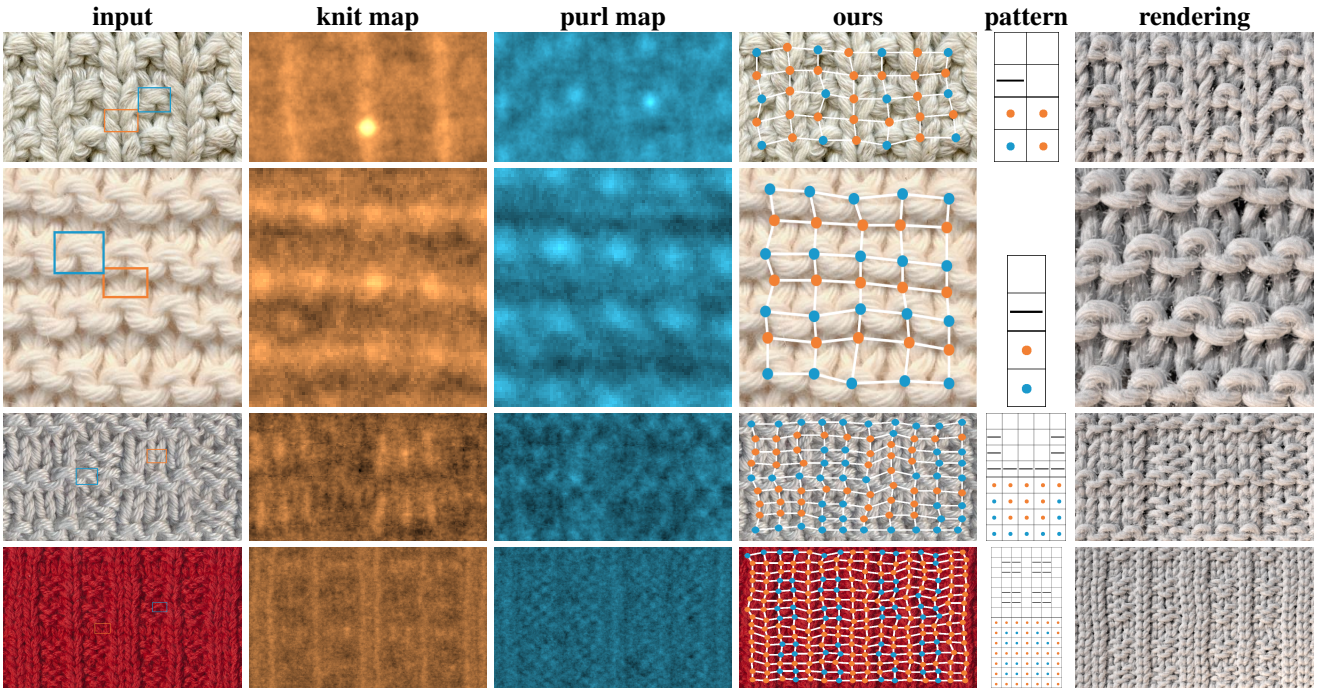


Figure 9: From left to right: input image, likelihoods for both stitch types, grid structure inferred via our approach and corresponding knitting instruction (empty cells represent knits and cells containing bars represent purls), as well as renderings. **Sample IDs 1, 2, 3, 4**.

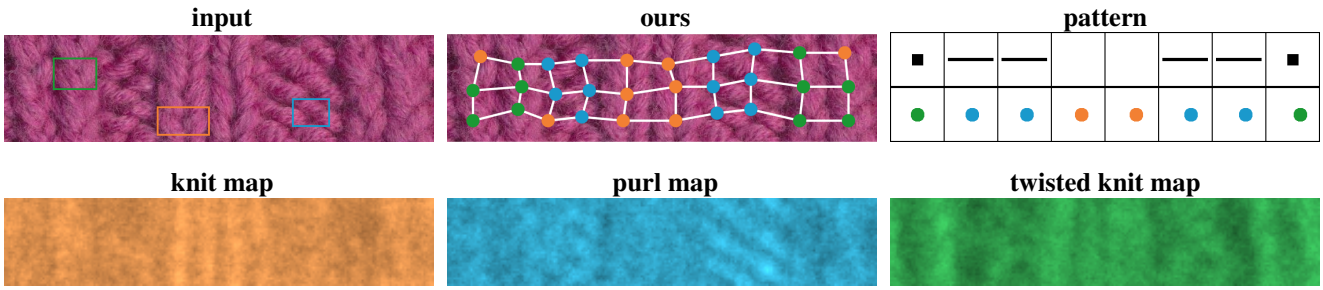


Figure 10: Exemplary results for a knitting pattern involving three different stitch types (**Sample ID 7**). Besides the input image with the user-provided stitch type selections, we show the grid structure inferred via our approach and the corresponding knitting instruction (empty cells represent straight knits, cells containing squares represent twisted knits and cells containing bars represent purls) (upper row). Furthermore, we show the likelihood maps for the individual stitch types (bottom row).